In Vivo Detection of Dysplastic Tissue by Raman Spectroscopy

ARTICLE *in* ANALYTICAL CHEMISTRY · JANUARY 2001

Impact Factor: 5.64 · DOI: 10.1021/ac000780u · Source: PubMed

8 AUTHORS, INCLUDING:

Tom C Bakker Schut
Erasmus MC
65 PUBLICATIONS **2,083** CITATIONS
SEE PROFILE

Max Jh Witjes
University of Groningen
101 PUBLICATIONS **1,413** CITATIONS
SEE PROFILE

Henricus J C M Sterenborg
Academisch Medisch Centrum Universiteit va…
255 PUBLICATIONS **5,896** CITATIONS
SEE PROFILE

Jan L N Roodenburg
University of Groningen, University Medical C…
223 PUBLICATIONS **4,792** CITATIONS
SEE PROFILE

Anal. Chem. **2000,** *72,* 6010−6018

In Vivo Detection of Dysplastic Tissue by Raman Spectroscopy

T. C. Bakker Schut,[†] M. J. H. Witjes,[‡] H. J. C. M. Sterenborg,[§] O. C Speelman,[§] J. L. N. Roodenburg,[‡] E. T. Marple,[⊥] H. A. Bruining,[†] and G. J. Puppels*,[†]

Erasmus Medical Center Rotterdam, Dr. Molewaterplein 50, 3015 GE, Rotterdam, The Netherlands, Department of Oral and Maxillofacial Surgery, University Hospital Groningen, P.O. Box 30.001, 9700 RB, Groningen, The Netherlands, Daniël den Hoed Kliniek, Groene Hilledijk 301, 3075 EA, Rotterdam, The Netherlands, Visionex, 430 Tenth Street, N.W., Suite N205, Atlanta, Georgia 30318

The detection of dysplasia and early cancer is important because of the improved survival rates associated with early treatment of cancer. Raman spectroscopy is sensitive to the changes in molecular composition and molecular conformation that occur in tissue during carcinogenesis, and recent developments in fiber-optic probe technology enable its application as an in vivo technique. In this study, the potential of Raman spectroscopy for in vivo classification of normal and dysplastic tissue was investigated. A rat model was used for this purpose, in which dysplasia in the epithelium of the palate was induced by topical application of the carcinogen 4-nitroquinoline 1-oxide. High quality in vivo spectra of normal and dysplastic rat palate tissue, obtained using signal integration times of 100 s were used to create tissue classification models based on multivariate statistical analysis methods. These were tested with an independent set of in vivo spectra, obtained using signal collection times of 10 s. The best performing model, in which signal variance due to signal contributions of the palatal bone was eliminated, was able to distinguish between normal tissue, low-grade dysplasia, and high-grade dysplasia/carcinoma in situ with a selectivity of 0.93 and a sensitivity of 0.78 for detecting low-grade dysplasia and a specificity of 1 and a sensitivity of 1 for detecting high-grade dysplasia/carcinoma in situ.

The transformation of normal tissue into a cancerous lesion is a slow process which involves alterations at the molecular level which, in later stages, are reflected in the morphology and tissue architecture. Usually different stages in the development of cancerous lesions can be recognized by histological evaluation. The presence and degree of certain histological features such as irregular stratification, loss of intercellular adherence and polarity as well as cellular features such as nuclear size and increased mitotic activity make up the difference between low-grade dysplasia, high-grade dysplasia, and carcinoma in situ.

Detection of dysplasia and early cancer is important because of the improved chances of treating the cancer successfully. Dysplasia is diagnosed by histopathologic classification and grading of tissue samples, which are usually obtained as biopsies. The number of tissue samples that can be obtained and investigated is limited. Moreover, in most cases, there exist no obvious visual clues that enable dysplastic tissue to be distinguished from normal tissue by the clinician taking the biopsies. Often biopsies are taken randomly. This results not only in high numbers of unnecessary biopsies (i.e., biopsies of normal tissue) but also in a significant risk of missing areas of dysplastic tissue.[1]

Fast, nondestructive optical in vivo detection of dysplasia will enable real-time guidance of the biopsy process. It would enable one to investigate many more tissue locations in the tissue and at the same time reduce the number of actual physical tissue samples that need to be evaluated by the pathologist because biopsies would be taken only from suspicious areas. Moreover, when the analysis can be made in real time, it can serve as a guidance tool for various other clinical interventions such as surgery or photodynamic therapy.[2,3]

A number of spectroscopic techniques are currently being investigated for application in in vivo detection of pre-malignant alterations in tissue.[4] Most research focuses on detecting the changes in intensity and/or spectral shape of (intrinsic) tissue fluorescence which are due to changes in tissue physiology during the neoplastic process. Sensitivities and specificities of over 0.90 have been reported in several studies.[5] Additionally, elastic light-scattering spectroscopy, which monitors changes in cell morphology and tissue structure, has been proven to be able to discriminate between normal and dysplastic tissue.[4,6,7]

* Address all correspondence to: G. J. Puppels, Ph. D., Erasmus University Hospital "Dijkzigt", Department of General Surgery, 10 midden, Dr. Molewaterplein 40, 3015 GD Rotterdam, The Netherlands. E-mail: Puppels@hlkd.azr.nl.

[†] Erasmus Medical Center Rotterdam.

[‡] University Hospital Groningen.

[§] Daniël den Hoed Kliniek.

[⊥] Visionex.

(1) Falk, G. W.; Rice, T. W.; Goldblum, J. R.; Richter, J. E. *Gastrointest. Endosc.* **1999**, *49* (2), 170−176.

(2) Barr, H. *Lancet* **1998**, *352*, 1242−1244.

(3) van den Boogert, J.; van Hillegersberg, R.; de Bruin R. F.; Tilanus, H. W.; Siersema, P. D.; Scand. J. *Gastroenterology* **1998**, *33*, 449−453.

(4) Bohorfoush, A. G. *Endoscopy* **1996**, *28*, 372−380.

(5) Wagnières, G. A.; Star, W. M.; Wilson, B. C. *Photochem. Photobiol.* **1998**, *68* (5), 603−632.

(6) Zonios, G.; Cothren, R.; Crawford, J. M.; Fitzmaurice, M.; Manoharan, R.; Van Dam, J.; Feld, M. S. *Ann. N. Y. Acad. Sci.* **1998**, *838*, 108−115.

10.1021/ac000780u CCC: $19.00
Published on Web 11/16/2000

Infrared spectroscopy is also widely used in characterization of tissue and in vitro detection of (pre)malignant changes.[8,9] However, application of infrared spectroscopy for in vivo detection of dysplastic changes is hampered by the fact that the penetration depth of infrared light is only a few micrometers.

Raman spectroscopy can detect the changes in molecular composition that accompany the neoplastic changes. Earlier work proved that cancerous tissue could be discriminated from normal tissue and pre-malignant tissue by in vitro Raman spectroscopy and multivariate statistical classification techniques.[10−17] Raman spectroscopy can be applied in vivo using special fiber optic probes, which can be optimized with respect to the size and location of the actual measurement volume in the tissue.[18,19] The feasibility of performing in vivo Raman spectroscopy in a clinical setting has recently been demonstrated, both during endoscopy.[20,21] Applicability of in vivo Raman spectroscopy in a clinical setting depends on the development of sensitive equipment and powerful spectral analysis to enable rapid signal collection and real-time extraction of clinically relevant parameters from these spectra. In this study we investigated the possibilities for in vivo classification of healthy and dysplastic tissue by NIR Raman spectroscopy. Using fiber-optic probes, in vivo spectra of the palatal tissue of rats were measured, in which dysplasia had been induced by topical application of the carcinogen 4-nitroquinoline 1-oxide (4NQO). The palates were measured after 9 weeks of 4NQO treatment, which resulted in low-grade dysplasia, and after 16 weeks of treatment, which resulted in high-grade dysplasia. Principal component analysis (PCA) followed by linear discriminant analysis (LDA) on a data set of high-quality palate spectra, measured in 100 s, was used to develop tissue classification models. An independent data set of palate spectra, measured in 10 s, was used to test the classification models.

MATERIAL AND METHODS

Raman Setup. For all in vivo measurements, 100 mW of 830-nm laser light from a model PI-ECL-830-500 diode laser (Process Instruments, Salt Lake City, UT) was used to illuminate the tissue. For the dysplasia study, an Enviva gaser-level 10-fiber-optic Raman probe (Visionex Inc, Atlanta GA) was used to guide the laser light to the tissue and to collect the Raman light. The principles and performance of this type of probe have been described in detail elsewhere.[18,22] Briefly, the probe consists of a central fiber (core diameter, 400 μm) for laser delivery and seven collection fibers (core diameter, 300 μm) around the central fiber. The central illumination fiber has an internal dielectric band-pass filter which transmits the wavelength of the laser light but blocks Raman signal generated by the laser light in the fiber material. The signal collection fibers have high-pass dielectric filters near the probe tip which transmit the collected Raman-scattered light of the tissue but block scattered laser light to prevent generation of Raman scattering in the collection-fiber material. The collection fibers are beveled at the probe end to achieve control over the actual measurement volume, that is, the overlap between the fields of view of the excitation fiber and the collection fibers. The gaser-level 10 probe collects a signal most efficiently at a distance of 100−600 μm from the probe tip end.[18] To achieve maximum signal collection efficiency at the palatal tissue surface, which is in contact with the probe tip during a measurement, a CaF_2 window of 200-μm thickness was used as a spacer between the probe tip and the tissue. A schematic drawing of the probe tip is given in Figure 1. A filter stage, which further suppresses the intensity of the scattered laser light, images the ends of the 7 collection fibers onto the 100-μm entrance slit of the spectrometer.[14]

An F/2 spectrometer, built in-house and equipped with a liquid nitrogen-cooled back-illuminated deep depletion CCD (charge-coupled device) camera (Princeton Instruments, Trenton, NJ), was used to record the spectra.[14] The Raman spectra collected by the 7 collection fibers were stored separately for wavenumber calibration and pretreatment before being added and analyzed.

Animal Experiments. *Carcinogen Treatment.* The experiments described in this paper were approved by the Internal Animal Care and Use Committee of the Erasmus University. Raman experiments were carried out on male Wistar rats (350−400 gr). Histological changes were induced in rat palate tissue by repeated (three times a week) topical application of the carcinogen 4-nitroquinoline 1-oxide (4NQO).[23] This carcinogen causes squamous cell carcinoma within a time scale of 5−7 months. During this period, neoplastic changes progress from low-grade dysplasia (LGD) to high-grade dysplasia (HGD) and carcinoma in situ (CIS), resulting ultimately in invasive tumor growth. The epithelial atypia index (EAI) was used as a qualitative

(7) Perelman, L. T.; Backman, V.; Wallace, M.; Zonios, G.; Manoharan, R.; Nusrat, A.; Shields, S.; Seiler, M.; Lima, C.; Hamano, T.; Itzkan, I.; Van Dam, J.; Crawford, J. M.; Feld, M. S. *Phys. Rev. Lett.* **1998**, *80*, 627−630.

(8) Jackson, M.; Mantsch, H. H. In *Biomedical Applications of Spectroscopy;* Clark, R. J. H., Hester, R. E., Eds.; John Wiley and Sons: Chichester, 1996; Chapter 5.

(9) Chiriboga, L.; Xie, P.; Yee, H.; Zarou, D.; Zakim, D.; Diem, M. *Cell. Mol. Biol.* **1998**, *44*, 219−229.

(10) Mahadevan-Jansen, A.; Richards-Kortum, R. *J. Biomed. Opt.* **1996**, *1*, 31−70.

(11) Mahadevan-Jansen, A.; Mitchell, M. F.; Ramanujam, N.; Malpica, A.; Thomsen, S.; Utzinger, U.; Richards-Kortum, R. *Photochem. Photobiol.* **1998**, *68* (1), 123−132.

(12) Mahadevan-Jansen, A.; Mitchell, M. F.; Ramanujam, N.; Utzinger, U.; Richards-Kortum, R. *Photochem. Photobiol* **1998**, *68* (3), 427−431.

(13) Manoharan, R.; Wang, Y.; Dasari, R. R.; Singer, S. S.; Rava, R. P.; Feld, M. S. *Lasers in the Life Sciences* **1995**, *6* (4), 217−227.

(14) Wolthuis, R.; Bakker Schut, T. C.; Caspers, P. J.; Buschman, H. P. J.; Römer, T. J.; Bruining, H. A.; Puppels, G. J. In *Fluorescent and Luminescent Probes for Biological Activity;* Mason, W. T., Ed.; Academic Press: London, 1999; Chapter 32.

(15) Boustany, N. N.; Crawford, J. M.; Manoharan, R.; Dasari, R. R.; Feld, M. S. *Lab. Invest.* **1999**, *79*, 1201−1214.

(16) Frank, C. J.; McCreery, R. L.; Redd, D. C. B. *Anal. Chem.* **1995**, *67* 7(5), 777−783.

(17) Hanlon, E. B.; Manoharan, R.; Koo, T. W.; Shafer, K. E.; Motz, J. T.; Fitzmaurice, M.; Kramer, J. R.; Itzkan, I.; Dasari, R. R.; Feld, M. S. *Phys. Med. Biol.* **2000**, *45* (2), R1−R59.

(18) Shim, M. G.; Wilson, B. C.; Marple, E.; Wach, M. *Appl. Spectrosc.* **1999**, *53* (6), 619−627.

(19) Puppels, G. J.; van Aken, T.; Wolthuis, R.; Caspers, P. J.; Bakker Schut, T. C.; Bruining, H. A. *Infrared Spectroscopy: New Tool in Medicine;* SPIE conference proceedings,vol. 3257; Mantsch, H. H., Jackson, M., Katzir, A., Eds.; Washington, 1998, 787−786.

(20) Shim, M. G.; Song, L. M.; Marcon, N. E.; Wilson, B. C. *Photochem. Photobiol.* **2000**, *72*, 146−150.

(21) Buschman, H. P.; Marple, E. T.; Wach, M. L.; Bennett, B.; Bakker Schut, T. C.; Bruining, H. A.; Bruschke, A. V.; van der Laarse, A.; Puppels, G. J. *Anal. Chem.* **2000**, *72*, 3771−3775.

(22) Puppels, G. J.; Bakker Schut, T. C.; Caspers, P. J.; Wolthuis, R.; van Aken, M.; Buschman, H. P. J.; van der Laarse, A.; Shim, M. G.; Wilson, B. C.; Bruining, H. A. *Handbook of Raman Spectroscopy*, 2000, In press.

(23) Nauta J. M.; Roodenburg J. L.; Nikkels P. G.; Witjes M. J.; Vermey, A. "Epithelial Dysplasia and Squamous Cell Carcinoma of the Wistar Rat Palatal Mucosa: 4NQO model.", *Head Neck* **1996**, *18*, 441−449.

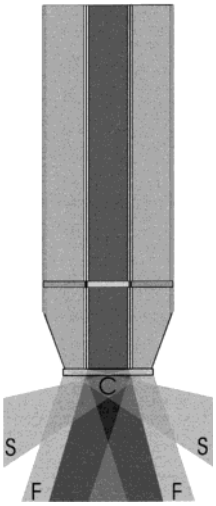

Figure 1. Schematic drawing of the fiber probe tip used in these experiments. The central illumination fiber has an internal dielectric band-pass filter and the signal collection fibers have high-pass dielectric filters near the probe tip. The collection fibers were beveled to maximize light collection from the first 100−600 μm. A CaF_2 window of 200-μm thickness was used as a spacer between the probe tip and the tissue. The cone of the central fiber (laser delivery) is depicted in dark gray. Each collection fiber has two collection cones, one forward viewing cone (F), and one sideward viewing cone (S). Most Raman signal comes from the area denoted by C, which combines high laser power with high collection efficiency.

histological measure for the degree of dysplasia.[24] It scores 13 individual features of epithelial dysplasia and ranges from 0 (no changes) to about 50 (CIS). In previous studies, it has been shown that there is a strong correlation between the duration of the 4NQO treatment and the EAI, which makes it a predictable model.[23] Photographs of typical examples of rat palates at different stages in the carcinogenic process are shown in panels A−F of Figure 2 (reproduced from).[25]

In panel A, the palate of a healthy rat is shown; a cross-section of the intermolar tissue is shown in panel B. The total thickness of the palate (keratin, epithelial and submucosal layer) tissue is about 500 μm.

In panel C, the palate of a rat with low-grade dysplastic tissue is shown. Dysplasia is clinically characterized by keratosis, which results in a rougher appearance of the mucosa. A cross-section of the low-dysplastic intermolar tissue is shown in panel D. Elongation of the rete ridges and increasing thickness of the keratin layer are the initial signs of dysplasia. At a higher magnification, slight basal cell hyperplasia, loss of polarity of the cells, and increased nucleo-cytoplasmatic ratio can be observed. The total thickness of the palate increases to 1000 μm. In panel E, a palate of a rat with high-grade dysplastic tissue is shown. The keratosis of the mucosa has changed further into a more disorganized aspect. The corresponding cross-section, shown in panel F, shows that the elongation of the rete ridges has progressed as well as the thickness of the keratin layer. At a higher magnification, cellular signs such as keratinisation below the keratin layer, severe basal cell hyperplasia, anisocytosis, loss of attachment, etc. can be observed.

Raman Experiments. Two series of Raman measurements were carried out. In total, the palates of 10 rats were measured. The first series of experiments was performed after 9 weeks of 4NQO-treatment with 3 rats that showed low-grade dysplastic palate tissue, and with 3 age-matched untreated rats (EAI = 2−5). The second series of Raman measurements was performed after 16 weeks of 4NQO-treatment with 2 rats that showed palate tissue with high-grade dysplasia/cancer in situ, and with 2 age-matched untreated rats.

The rats were anesthetized using ether. During the measurements, the rats were in supine position with their heads immobilized in a stereotactical instrument. For the in vivo collection of palate epithelium Raman spectra, the modified gaser-level 10-fiber probe was kept in contact with the tissue. Two different collection times were used during the Raman measurements. High-quality spectra, obtained in 100 s were used for development of the multivariate statistical tissue classification models (see below). Spectra with a lower signal-to-noise ratio were obtained in 10 s and were used for testing these models. For each rat, 4 or 5 measurements of 100 s and 3−5 measurements of 10 s were performed, all at different locations on the palate, both on and between the ridges. Total measurement time per rat was about 15 min. All rats were sacrificed immediately after the Raman measurements, and the palates were histologically examined following procedures described earlier.[23]

In the first series of measurements, 13 model spectra and 9 test spectra were obtained of both normal palates and low-grade dysplastic palatal tissue. In the second series of measurements, 10 model spectra and 10 test spectra were obtained of both normal and high-grade dysplastic palatal tissue.

Spectral Analysis. All spectral analysis software was developed in a Matlab environment (Matlab 5.3: The MathWorks, Inc., Natick, MA) using the multivariate statistical analysis toolbox PLS-toolbox 2.0.0c (Eigenvector Research, Inc., Manson, WA).

Pretreatment of Spectra. The spectra of the different collection fibers were calibrated separately using Raman calibration standards as described earlier.[14] The spectral resolution is about 7 cm^{-1}. All spectra were corrected separately for the wavelength-dependent sensitivity of the setup, which was determined using a calibrated tungsten band lamp.[14] The fused-silica Raman signal generated in the unfiltered segments of the central illumination fiber and the signal collection fibers was subtracted from the tissue spectra. After this, the spectra from the different collection fibers were added. To enhance the Raman features and reduce the influence of slowly varying backgrounds, the resulting spectra were Savitzky−Golay differentiated using a smoothing window of 15 wavenumbers. Subsequently, the spectra were scaled to have zero mean and unit variance [auto-scaling or standard normal variate (SNV) scaling].[16]

Tissue Classification Models. Multivariate statistical classification models were built using the basis set of high-quality (100 s) spectra as follows. Clear outliers were removed from the model data set. These were defined as spectra obtained from the same rat palate that do not fall within a boundary of 20 times the standard deviation from the mean spectrum of that palate. Principal component analysis (PCA) was used on the model set

(24) Smith, C. J.; Pindborg J. J. *Histological Grading of Oral Epithelial Atypia by the Use of Photographic Standards*; C. Hamburger: Copenhagen, 1969.

(25) Witjes, M. J. H. *Photodynamic Therapy and Fluorescence Localisation of Experimental Ora Dysplasia and Squamous Cell Carcinoma.* Ph.D. Thesis, University of Groningen, The Netherlands, 1997, Chapter 1.

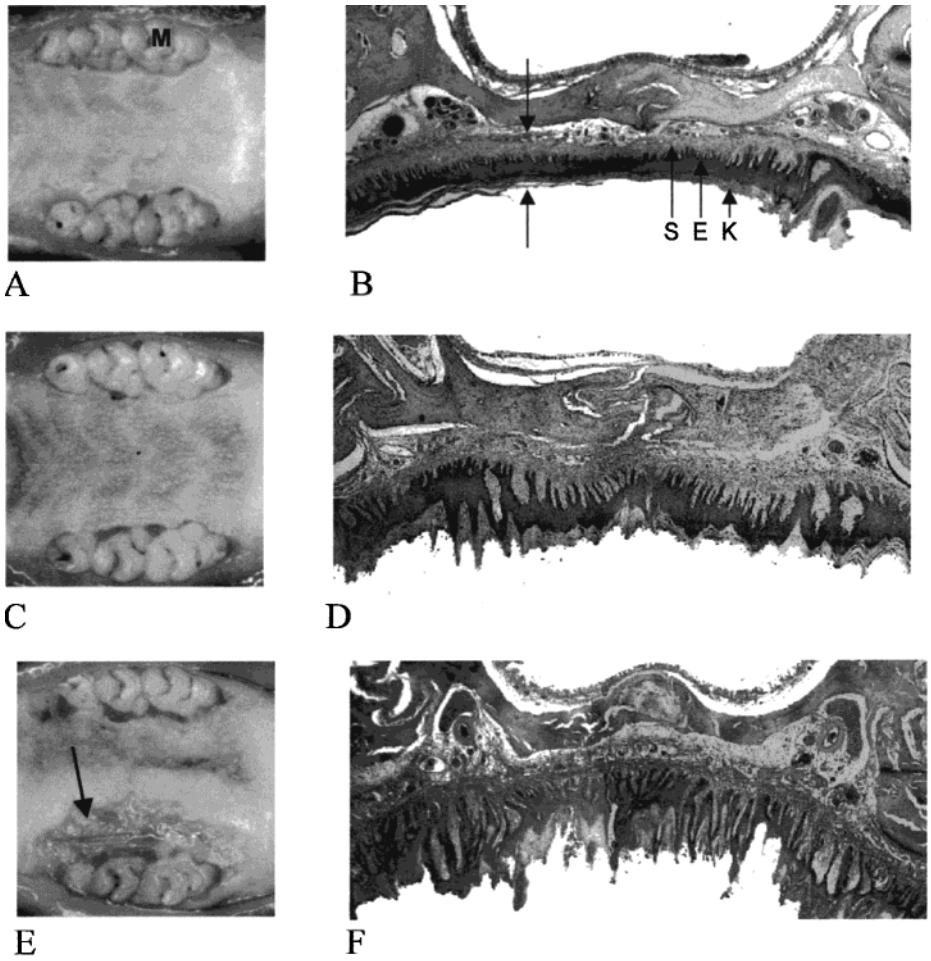

Figure 2. Photographs illustrating the neoplastic progression in palates of 4NQO− treated rats. A: Macroscopic appearance of the palatal mucosa of a healthy rat. The anterior side of the head is located at the right. Raman spectra were collected throughout the region between the two rows of molars (M). B: Hematoxilin and eosin (H&E)-stained section of the palatal mucosa of a healthy rat. The total thickness of the palate [keratin (K), epithelial (E), and submucosal (S) layer] tissue, indicated by the two arrows on the left side, is about 500 μm. C: Macroscopic appearance of the palatal mucosa with low-grade dysplasia. The appearance of the mucosa is more rough due to keratosis. D: H&E-stained section of the palatal mucosa with low-grade dysplasia. Elongation of the rete ridges and increasing thickness of the keratin layer are the initial signs of dysplasia. The total thickness of the palate (keratin, epithelial, and submucosal layer) tissue is about 1000 μm. E: Macroscopic appearance of the palatal mucosa of a rat with high-grade dysplasia/carinoma in situ. The arrow denotes an area with squamous cell carcinoma. F: H&E-stained section of the palatal mucosa of a rat with high-grade dysplasia. The elongation of the rete ridges has progressed, as well as the thickness of the keratin layer. In this section, the area with squamous cell carcinoma is not shown.

to orthogonalize and reduce the number of parameters needed to represent the variance in the spectral data set. Only principal components (PCs) that accounted for more than 1% of the variance in the data set were retained. A two-sided t-test was used to individually select those PCs that showed the highest significance in discriminating the different tissue classes. The number of PCs that was used as input for the LDA model was kept at least two times smaller than the number of spectra in the smallest model group to prevent overfitting in the LDA model.

The scores of the model spectra on these PCs, which represent most of the useful variance in the data-set, were used as input for an LDA model. LDA yields $n-1$ linear discriminants (LDs) that best separate n given groups by finding the directions in spectral space that yield the highest ratios between inter- and intragroup distances.[26]

Raman spectra were obtained at random locations on the palates. The locations for which EAI scores were determined did not exactly match the locations of the Raman measurements. Therefore, the highest EAI score found during the histological evaluation of the palates was used to develop the tissue classification models. These EAI scores may, therefore, slightly overestimate the degree of dysplasia at the locations of the Raman measurements. Spectra of rats with a maximum EAI of 2−5 were classified as "normal", spectra of rats with a maximum EAI of 27−31 were classified as low-grade dysplasia (LGD), and spectra of rats with an EAI of >40 were classified as high-grade dysplasia/carcinoma in situ (HGD/CIS). There were no rats with an EAI between 6 and 26 and with an EAI between 32 and 40. Although the pathology of these chemically induced cancers is quite homogeneous, there can still exist patches of normal tissue within the low-grade dysplastic epithelium or patches of low-grade dysplastic tissue in the epithelium graded as high-grade dysplastic/carcinoma in situ. These can lead to a wrong labeling for some spectra and, therefore, cause errors in the LDA model.

The tissue classification models were tested using the independent data set of 10 s spectra. These prediction spectra were

(26) Tabachnick, B.; Fidell, L. *Using Multivariate Statistics*, 3th ed.; HarperCollins Publishers: New York, 1989.

first projected on the PCA model, and the scores of these prediction spectra on the PC's were subsequently projected on the LDA model to yield a classification prediction.

Vector Correction. In a recent paper by our group, a nonsubjective method was introduced to eliminate signal variance in a spectral database that is due to varying signal contributions of known origin.[27] This procedure, coined vector correction, was used here to eliminate signal variance due to varying signal contributions of the palatal bone in Raman spectra from rat palates. In short, the two spectra are represented as vectors in an *n*-dimensional space where *n* is the spectral range. The epithelium vector is then decomposed in a vector parallel to the bone spectrum and a vector perpendicular to the bone spectrum. The vector perpendicular to the bone spectrum will be independent of the amount of bone signal originally present in the palatal epithelium Raman signal. This procedure does not claim to exactly subtract the amount of bone signal present in the palatal epithelium spectrum, and care should be taken if the purpose is to draw conclusions about the molecular composition of tissue or changes therein due to disease, after vector correction of the spectra. However, this is not of importance when developing classification models.

Here we applied the vector correction procedure on the scores of the PCA model. The scores of a spectrum also represent a vector in an *n*-dimensional space where *n* is now the number of PCs. The advantage of applying the vector correction procedure in PC space is that one can make use of the signal-averaging effects of PCA by not including the low eigen-value PCs that capture little variance and contain mostly noise.

RESULTS

After application of 4NQO for nine weeks in vivo, Raman spectra of the palates of three rats were collected. Pathological evaluation of the palate tissue after the Raman experiments showed that the palate epithelium of these rats was low-grade dysplastic (EAI of 27−31). Raman spectra of the palates of an age-matched control group of three untreated rats were also collected. For each rat, at least 4 spectra were obtained with a 100-s signal collection time and 3 spectra with a 10-s signal collection time, at different locations of the palate. Raman signal generated in the fiber-optic Raman probe itself and any fluorescence background signal were subtracted from all recorded palate-spectra, which were subsequently auto-scaled. Typical spectra of normal rat palate tissue, measured in 100 s and 10 s are shown in Figure 3. The spectra were calibrated and corrected for contributions from the emission and collection fibers, as described above, and finally, a sixth-order polynomial was subtracted from the spectra to remove any remaining non-Raman background. It should be noted that the spectra that are used in the LDA model were not corrected for the remaining background; only a first-order derivative was used to reduce the influence of the background. The mean 100-s spectra of both groups are shown in Figure 4.

After 16 weeks of 4NQO treatment in vivo, Raman spectra of the palates of 2 rats were collected. Pathological evaluation of the palate tissue after the Raman experiments showed that the palate epithelium of these rats was high grade dysplastic/carcinoma in situ (EAI >40) Again, Raman spectra of the palates of an age-matched control group of two untreated rats were also collected. For each rat, 5 100-s spectra and 5 10-s spectra were obtained at different locations on the palate. The mean spectra of these two groups are shown in Figure 4. For reference, a spectrum of palatal bone, which in normal palate is located just 500 μm below the surface of the epithelium, is also given in Figure 4. As can be seen from Figure 4, the spectra of normal rat palate tissue is dominated by the contributions of the palatal bone. During the dysplastic process, the epithelial tissue thickens, which causes the relative signal contribution of bone to diminish.

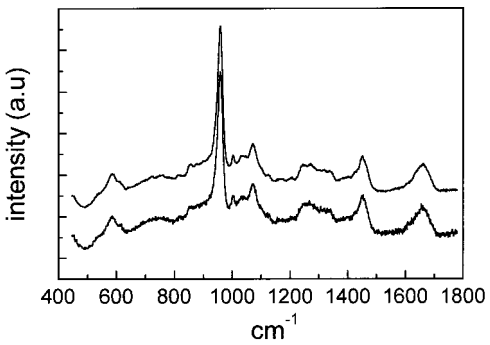

Figure 3. Typical Raman spectra of normal rat palate measured in 100 s (upper spectrum) and 10 s (lower spectrum). The spectra were corrected for signal contributions from the fiber optic probe material and a fluorescence background fluorescence background was subtracted by means of fitting the baseline with a sixth-order polynomial.

Model 1. An LDA model for tissue classification on the basis of the in vivo Raman spectra was developed. The auto-scaled first-order derivatives of the 100-s spectra were used as the basis for the model. Four spectra out of 46 were identified as clear outliers and were removed from the model data set. The four removed spectra were all of normal tissue, and all were from different rats. They were rejected because of a markedly lower signal intensity and a relatively high background signal, which resulted in a poor signal-to-noise ratio. The probable cause for this is that the probe was not in close contact with the tissue. From the remaining 42 model spectra, 19 were of normal tissue, 13 spectra were of LGD, and 10 spectra were obtained of HGD. PCA was used to obtain a reduced number of orthogonal variables for the model spectra. The scores on the first four PCs, which showed the highest significance in discriminating the different tissue classes and together accounted for 96% of the total variance in the model data set, were selected as input for the LDA model.

In the upper part of Figure 5, a scatter plot is shown of the scores of all model spectra obtained by projecting the model spectra onto the two discriminants generated by the model. Three different groups can be distinguished, although there is some overlap between the spectra of normal tissue and low-grade dysplastic tissue. The spectra of normal tissue (light gray circles) are low in LD 1 and high in LD 2, the LGD spectra (dark gray triangles) are low in LD 1 and low in LD 2, and the HGD-spectra (black squares) are high in LD 1 and indefinite in LD 2. The projection of a pure-bone spectrum is also shown (cross).

This LDA-model was evaluated using a leave-one-out cross-validation on all model spectra. The results of the cross-validation are given in Table 1. The model specificity for detecting HGD is 0.97 with a sensitivity of 0.80; for LGD-detection, the model specificity is 0.93, and sensitivity is 0.77.

(27) Maquelin, K.; Choo-Smith, L.-P.; van Vreeswijk, T.; Endtz, H. Ph.; Smith, B.; Bennett, R.; Bruining, H. A.; Puppels, G. J. *Anal. Chem*. **2000**, *72* (1), 12−19.

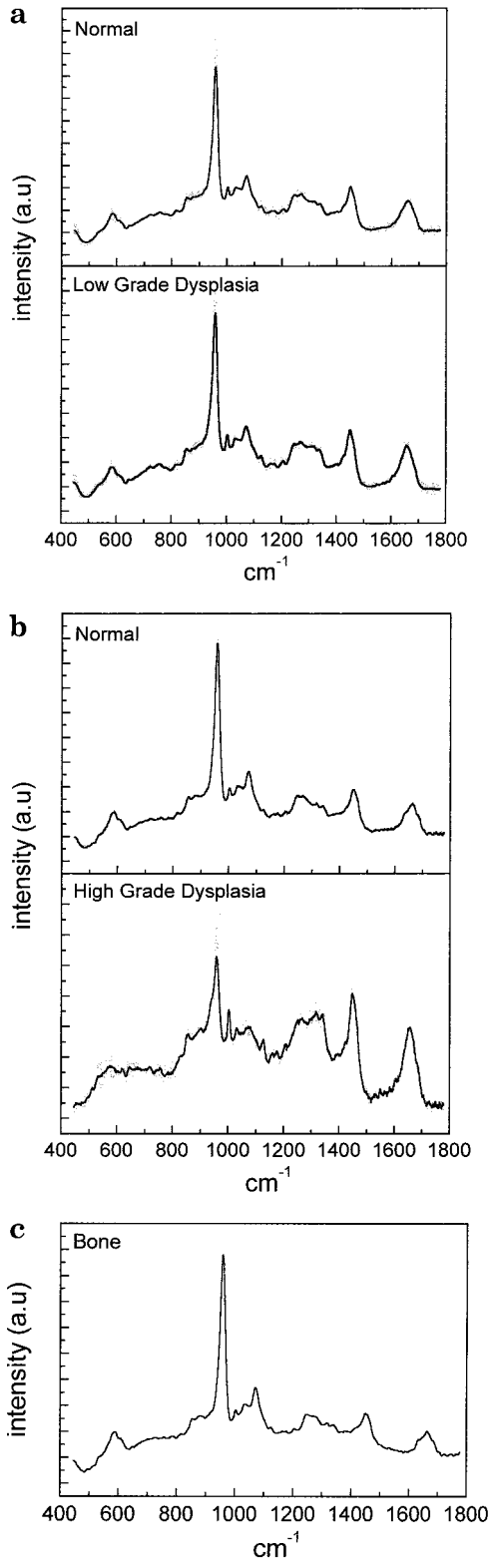

Figure 4. Mean in vivo spectra of normal, low-grade, and high-grade dysplastic rat palate tissue and the spectrum of the underlying palatal bone. The gray area represents the variance within one standard deviation from the mean. The spectra were corrected for signal contributions from the fiber-optic probe material and a fluorescence background fluorescence background was subtracted by means of fitting the baseline with a sixth-order polynomial. A: Mean in vivo spectra of the first measurement series. B: Mean in vivo spectra of the second measurement series. C: Ex vivo spectrum of rat palatal bone.

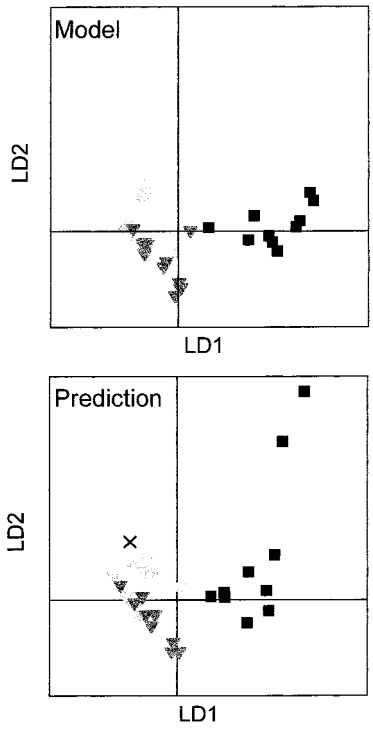

Figure 5. Scores on LDA model 1 for both the 100-s model spectra (upper part) and the 10-s prediction spectra (lower part) on the model discriminants shown in Figure 4. The normal spectra (light gray circles) are low in LD1 and high in LD2, the low-grade dysplastic spectra (dark gray triangles) are low in LD1 and low in LD2, and the high-grade dysplastic spectra (black squares) are high in LD1 and indefinite in LD2. The projection of a pure-bone spectrum is also shown (black cross).

Table 1. Classification of the Model Spectra Using LDA Model 1

	pathology			
Raman	HGD	LGD	normal	total
HGD	8	1	0	9
LGD	1	10	1	12
normal	1	2	18	21
total	10	13	19	42

Table 2. Classification of the Test Spectra Using LDA Model 1

	pathology			
Raman	HGD	LGD	normal	total
HGD	9	0	0	9
LGD	1	6	2	9
normal	0	3	17	20
total	10	9	19	38

The model was used for prediction of an independent test set of 38 spectra, measured in 10 s on the same rat palates. The projections of the test spectra on the model are shown in the lower part of Figure 5. The results of the classification of these test spectra are given in Table 2. The prediction specificity for detecting HGD is 1 with a sensitivity of 0.9, and the prediction specificity for LGD is 0.9 with a sensitivity of 0.67.

Model 2. Although the results of the classification with model 1 show that it is possible to discriminate between normal tissue,

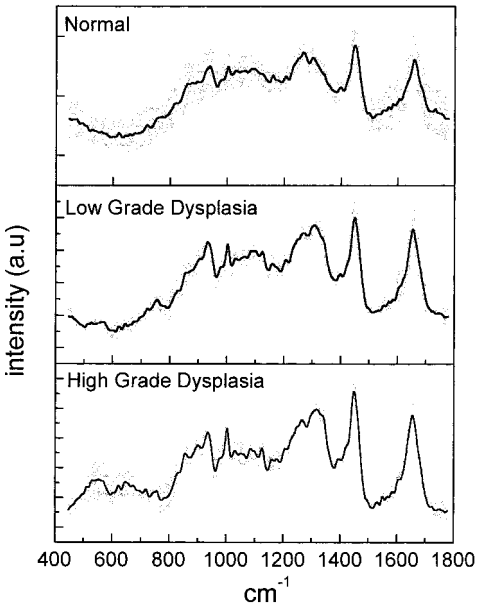

Figure 6. Mean in vivo model spectra of normal, low-grade dysplastic, and high-grade dysplastic rat palate tissue after correction for the variance that could be attributed to bone-signal contributions. The gray area represents the variance within one standard deviation from the mean.

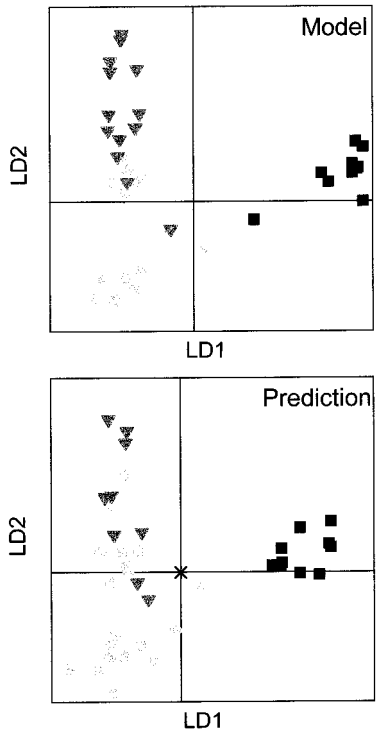

Figure 7. Scores on LDA model 2 for both the 100-s model spectra (upper part) and the 10-s prediction spectra (lower part) on the model discriminants shown in Figure 7. All spectra were corrected for the variance that could be attributed to bone. The normal spectra (light gray circles) are low in LD1 and LD2, the low grade dysplastic spectra (dark gray triangles) are low in LD1 and high in LD2, and the high grade dysplastic spectra (black squares) are high in LD1 and indefinite in LD2. The projection of a pure-bone spectrum is also shown (black cross).

low-grade dysplasia, and high-grade dysplasia, the relative amount of signal received from the palatal bone plays a role in the linear discriminant model. The projection of a pure-bone Raman spectrum on the LDA model, as depicted in the lower part of Figure 5B by a cross, has a low LD1 score, which separates normal from HGD, and a high LD2-score, which separates normal from LGD. The spectrum of normal rat palate is dominated by the signal of the bone under the palate tissue. In the case of dysplasia, the epithelium thickens, and therefore, the signal contribution of bone to the measured spectra decreases. This can be used to discriminate between normal and dysplastic tissue, but the resulting model is probably not very robust with respect to other (pathological) causes for thickening of the epithelium. Therefore, we eliminated signal variance that can be attributed to bone from the classification model.

This was achieved by projecting the PCA scores of the in vivo model spectra onto the PCA scores of the Raman spectrum of pure bone and subtracting these projections from the original PCA scores by using a vector procedure, briefly explained in the materials and methods section and described in more detail elsewhere.[27] After application of this method, only the part of the spectrum that is perpendicular to the bone spectrum is retained, and all signal contributions that can be attributed to bone are effectively removed. The corrected scores were subsequently autoscaled to ensure equal contribution of all spectra to the LDA model.

In Figure 6, the means of the bone-corrected spectra are shown for the three types of tissue.

As can be seen, the dominant hydroxy-apatite peak of bone at 960 cm^{-1} has disappeared from all the spectra.

A second LDA model was built using the bone signal-corrected model scores. The scores on the first three PC s, accounting for 95% of the total variance in the model data set after the bone correction, were selected as input for the LDA model. In Figure 7A, a scatter plot of the scores of all model spectra is shown. It was obtained by projecting the bone-corrected model spectra onto these two discriminants. The three different groups can again be discriminated: the spectra of normal tissue (circles) are low in LD1 and LD2, the spectra of low-grade dysplasia are low in LD1 and high in LD2, and the spectra of high-grade dysplasia (squares) are high in LD1 and indefinite in LD2. Of course in this case, the projection of a pure-bone Raman spectrum (cross) that has received the same pretreatment as the other spectra is situated in the origin of the plot, illustrating the fact that the amount of bone signal present in the raw data no longer plays a role in the tissue classification model.

The bone-corrected LDA model was evaluated using a leave-one-out cross-validation on all model spectra. The results of this cross-validation are given in Table 3. The specificity and sensitivity of the model for HGD are 1 and 0.9 respectively; for LGD, specificity is 0.93, and sensitivity is 0.85.

The bone-corrected model was used for the prediction of an independent test set of 10-s spectra, which were also corrected for bone signal contributions. The projections of these test spectra on the model are shown in Figure 7B. The results of the classification of the test spectra are given in Table 4. Prediction specificity and sensitivity for HGD within the bone signal-corrected model are 1. Prediction specificity and sensitivity for LGD are 0.93 and 0.78, respectively.

Table 3. Classification of the Model Spectra Using LDA Model 2

	pathology			
Raman	HGD	LGD	normal	total
HGD	9	0	0	9
LGD	0	11	2	13
normal	1	2	17	20
total	10	13	19	42

Table 4. Classification of the Test Spectra Using LDA Model 2

	pathology			
Raman	HGD	LGD	normal	total
HGD	10	0	0	10
LGD	0	7	2	9
normal	0	2	17	19
total	10	9	19	38

DISCUSSION

Disease leads to changes in the molecular composition of tissue, and one may assume that such changes occur simultaneously or even precede changes in cell morphology and tissue structure. It follows that techniques that can provide information about these changes in molecular composition may constitute a suitable basis for the development of clinical tools aimed at early detection of disease. The pre-malignant stages in epithelial tumor development occur in the most superficial cell layers. Only optical techniques can provide the spatial resolution to specifically target these layers. Raman spectroscopy is an optical technique that provides a highly specific spectroscopic fingerprint of the molecular composition of a tissue, and recent in vitro studies have provided ample evidence that it enables one to distinguish normal tissue from (pre)malignant tissues.[10−17] The aim of this study was to test whether in vivo application of Raman spectroscopy for the purpose of detecting epithelial dysplasia is feasible at the technological state of the art.

The use of Raman spectroscopy for in vivo detection of dysplasia in a clinical setting will depend on the feasibility of measuring recognizable Raman spectra in a few seconds using fiber optic probes. Here we studied this feasibility by classifying normal and dysplastic tissue on the basis of in vivo Raman spectra that were measured in 10 s, using a multivariate statistical LDA model, based on spectra that were measured in 100 s. The spectra were obtained from normal and dysplastic rat palate tissue using a dedicated fiber optic probe.

The results of this in vivo study are very promising. Although the data set is limited in size, the results show for the first time that it is possible to detect high-grade dysplasia in vivo within a 10-s measurement and with a high sensitivity and specificity. Both of the LDA models show some overlap between the normal and low-grade dysplastic spectra. This is probably caused by the fact that the locations of the Raman measurements and the histological characterization of the tissue could not be exactly matched. Therefore, the Raman spectra obtained from a rat were assigned according to the maximum degree of dysplasia encountered on that rat's palate. The difference between Raman spectra of normal tissue and of high-grade dysplastic tissue is to a large extent caused by the relative amounts of epithelial tissue and bone that are present in the measuring volume, as can be seen from Figure 3. The spectrum of normal tissue is dominated by the spectral features of bone. Although the fiber-optic Raman probe was optimized to collect signal from the first few hundred μm of tissue, it also collects signal from deeper tissue layers, that is, the palatal bone, which is a relatively strong Raman scatterer. The dysplastic palate epithelium thickens, which leads to a relative decrease in bone signal contributions.

The results of LDA model 1 show that the projection of a Raman spectrum of pure bone onto the LDA model in Figure 4C is not located at the origin of the LDA plane but near the group of spectra from normal palate tissue, which are dominated by the contributions of the palatal bone. This shows that the Raman signal contributions of bone to the spectra do influence the tissue classification model. Because the signal contributions of bone can obscure the relevant information (namely, the difference in epithelial molecular composition) and, moreover, would probably make the classification model vulnerable to other causes of epithelial thickening, we eliminated the variance in the spectral database that can be attributed to varying bone Raman signal contributions. This was achieved by correcting the spectra in principal component space using a vector-correction procedure, which is described in the material and methods section.

The second LDA model, which used the bone signal-corrected PC scores as input, yields even slightly better classification results, both for the model spectra and for the independent test spectra, which shows that although it is a prominent feature in the spectra, the bone signal is not needed to distinguish between normal tissue, LGD, and HGD.

Autofluorescence in the same animal model as measured by van den Akker et al.[28] shows a small but distinct peak at 635 nm that is caused by porphyrins occurring in the tissue. This peak increases in cancerous tissue, but in the present model it did not increase at 6 or 12 weeks of treatment. At 18 weeks, there is a dramatic increase that would allow reliable diagnosis. Another study on optical detection of chemically induced cancers in the oral cavity using autofluorescence was performed on the hamster cheek pouch.[29] In this model there was a slight but significant increase in the protoporphyrin fluorescence peak in premalignant lesions and, again, a much more dramatic one in clearly visible carcinomas. It appears that the Raman spectroscopy is capable of detecting these lesions much earlier in their development.

An advantage of using multivariate statistical analysis to create tissue classification models is that they become fairly insensitive to noise due to the inherent signal-averaging effects of these methods.[30] This permits the use of relatively low signal-to-noise spectra for classification prediction, which means signal collection times can be kept short. As can be seen in Figures 4 and 6, the spread in discriminant scores of the model data (100-s signal collection) is about equal to that of the prediction set (10-s signal collection).

(28) van den Akker, J. T. H. M.; Speelman, O. C.; van Staveren, H. J.; Moore, A. L.; Moore, T. A.; Gust, D.; Star W. M.; Sterenborg, H. J. C. M. *J Photochem. Photobiol.* **2000**, *54*, 108−115.

(29) van der Breggen, E. W. J.; Rem, A. I.; Christian, M. M.; Yang, C. J.; Calhoun, K. H.; Sterenborg, H. J. C. M.; Motamedi, M. *IEEEJ Spec. Topics in Q E* 2 **1997**, 997−1007.

(30) Workman, J. J., Jr.; Mobley, P. R.; Kowalski, B.; Bro, R. *Applied Spectroscopy Reviews* **1996**, *31*, 73−124.

A disadvantage of using LDA, or any other nonobjective classification method, is the limitation on the number of parameters that can be used as input to the model to prevent overfitting of the spectral database in the model.[31] The number of parameters needed to describe the spectral variance of the data set was reduced by first applying a PCA. This method presents mutually orthogonal spectral variance components in descending order of importance. However, these are not necessarily optimal for discrimination of the different tissue classes. The useful information is generally distributed over a number of PCs. For all of our LDA models, the discriminative information was located in the first 3−4 PCs, which represented more than 95% of the variance in the data set. Therefore, in the LDA models, the number of input variables was >2 times smaller than the number of spectra in the smallest group, which is the HGD group with 10 spectra. The tests of the models with an independent set of (10-s) spectra yielded similar classifications and distributions of LDA scores as obtained for the model spectra, which indicates that there was, indeed, no overfitting of the dataset of spectra used to develop the classification model.

CONCLUDING REMARKS

In the present study, fiber-optic probes where used that were optimized for Raman signal collection close to the probe surface, but they nevertheless also collected signal from deeper tissue layers, in particular the palatal bone. The vector correction method was successful in eliminating the influence of the presence of this bone Raman signal. However it would be preferable to further optimize the fiber-optic probe in order to eliminate signal contributions from deeper tissue layers. We are currently investigating a number of approaches to realize this.

The spectra that were used to test the tissue classification models were obtained using a signal collection time of 10 s. A further reduction of the measurement time to 1−2 s would be required for most clinical applications.

The signal throughput of the current setup leaves room for such improvement so that we conclude that from a technological point of view, in vivo detection of epithelial dysplasia by Raman spectroscopy is feasible. Future studies will have to make clear for which applications Raman spectroscopy has advantages over other (optical) techniques such as fluorescence (spectroscopic) methods, elastic light-scattering spectroscopy and optical coherence tomography.

ACKNOWLEDGMENT

The authors express their gratitude to the Dutch Foundation for Scientific Research (NWO, Grant No. 910-38-055), the Dutch Cancer Foundation (Grant No. DDHK 95-1062), and to RENISHAW, Inc. (Wotton under Edge, U.K.) for financial support of this work. We thank M. van Aken for expert assistance during the in vivo animal experiments

Received for review July 7, 2000. Accepted October 3, 2000.

AC000780U

(31) Peduzzi, P.; Concato, J.; Kemper, E.; Holford, T. R.; Feinstein, A. R. *J. Clin. Epidemiol.* **1996**, *49*, 1373−1379.